JGP Journal of General Physiology

COMMUNICATION

Piezo2 interacts with E-cadherin in specialized gastrointestinal epithelial mechanoreceptors

Arnaldo Mercado-Perez[1,2,3], Jeric P. Hernandez[1,3,4], Yaroslav Fedyshyn[3], Anthony J. Treichel[6], Vikram Joshi[1,3], Kimberlee Kossick[4], Kalpana R. Betageri[3], Gianrico Farrugia[1,3,4], Brooke Druliner[3,4,5], and Arthur Beyder[1,3,4]

Piezo2 is a mechanically gated ion channel most commonly expressed by specialized mechanoreceptors, such as the enteroendocrine cells (EECs) of the gastrointestinal epithelium. A subpopulation of EECs expresses Piezo2 and functionally resembles the skin's touch sensors, called Merkel cells. Low-magnitude mechanical stimuli delivered to the mucosal layer are primarily sensed by mechanosensitive EECs in a process we term "gut touch." Piezo2 transduces cellular forces into ionic currents, a process that is sensitive to bilayer tension and cytoskeletal depolymerization. E-cadherin is a widely expressed protein that mediates cell–cell adhesion in epithelia and interacts with scaffold proteins that anchor it to actin fibers. E-cadherin was shown to interact with Piezo2 in immortalized cell models. We hypothesized that the Piezo2–E-cadherin interaction is important for EEC mechanosensitivity. To test this, we used super-resolution imaging, co-immunoprecipitation, and functional assays in primary tissues from mice and gut organoids. In tissue EECs and intestinal organoids, we observed multiple Piezo2 cellular pools, including one that overlaps with actin and E-cadherin at the cells' lateral walls. Further, E-cadherin co-immunoprecipitated with Piezo2 in the primary colonic epithelium. We found that E-cadherin knockdown decreases mechanosensitive calcium responses in mechanically stimulated primary EECs. In all, our results demonstrate that Piezo2 localizes to the lateral wall of EECs, where it physically interacts with E-cadherin and actin. They suggest that the Piezo2–E-cadherin–actin interaction is important for mechanosensitivity in the gut epithelium and possibly in tissues where E-cadherin and Piezo2 are co-expressed in epithelial mechanoreceptors, such as skin, lung, and bladder.

Introduction

Epithelial cells form barriers between outside and inside. In many organs, the epithelial layer is critical to sense luminal mechanical events, such as filling (Marshall et al., 2020) and shear stress (Wang et al., 2016; Zeng et al., 2018). Specialized mechanoreceptors are mechanosensitive cells that interpret forces at the barrier and initiate downstream physiologic responses (Mercado-Perez and Beyder, 2022; Ranade et al., 2014; Woo et al., 2014; Fettiplace, 2017; Fettiplace et al., 2022; Lembrechts et al., 2012; Nonomura et al., 2017). Epithelial mechanoreceptors are tightly embedded into multicellular epithelial layers stitched from single cells using junctional proteins, such as E-cadherin. These junctional complexes can also participate in force sensation and transmission (Lecuit and Yap, 2015), potentially contributing to the function of the specialized mechanoreceptors.

Mechanical cues in the gastrointestinal (GI) tract range from exogenous, such as meals filling the stomach (Umans and Liberles, 2018), to endogenous, like shear stress exerted by moving contents (Beyder, 2019; Mercado-Perez and Beyder, 2022). Mechanical activity in the gut lumen, through stimulation of the mucosal layer, leads to the release of serotonin (5-hydroxytryptamine, 5-HT) (Bulbring and Crema, 1959) via a mechanosensitive subpopulation of 5-HT-releasing cells known as enterochromaffin (EC) cells (Wang et al., 2017; Alcaino et al., 2018). These belong to the wider population of epithelial mechanosensitive enteroendocrine cells (EECs) which release a range of signaling molecules that modulate gut function (Billing et al., 2019; Beumer et al., 2020).

Mechanosensitive EECs are characterized by the expression of Piezo2, which they require to convert mechanical stimuli into signaling molecule release (Alcaino et al., 2018; Billing et al., 2019). Piezo1 and 2 are mechanically gated non-selective cation channels (Coste et al., 2010). Piezo2 specifically may function as

[1]Enteric NeuroScience Program (ENSP), Mayo Clinic, Rochester, MN, USA; [2]Medical Scientist Training Program (MSTP), Mayo Clinic, Rochester, MN, USA; [3]Department of Physiology and Biomedical Engineering, Mayo Clinic, Rochester, MN, USA; [4]Division of Gastroenterology and Hepatology, Department of Medicine, Mayo Clinic, Rochester, MN, USA; [5]Department of Biochemistry and Molecular Biology, Mayo Clinic, Rochester, MN, USA; [6]Stowers Institute for Medical Research, Kansas City, MO, USA.

Correspondence to Arthur Beyder: beyder.arthur@mayo.edu

This work is part of a special issue on "Structure and Function of Ion Channels in Native Cells and Macromolecular Complexes."

a multimodal molecular force sensor. Piezo2 currents are sensitive to lipid membrane tension (Haselwandter et al., 2022; Yang et al., 2022). Additionally, disruption of the actin cytoskeleton with cytochalasin D or latrunculin A decreases force-dependent Piezo2 currents in cultured cell models and dorsal root ganglia neurons (Eijkelkamp et al., 2013; Jia et al., 2016; Verkest et al., 2022). While the molecular details of Piezo2 tethering remain to be elucidated, both intra- and extracellular subdomains likely mediate its cytoskeletal sensitivity. Deletion of the intracellular-facing intrinsically disordered region 5 (IDR5) from Piezo2 eliminates the channel's sensitivity to cytochalasin-induced actin depolymerization (Verkest et al., 2022). The extracellular Piezo2 cap domain modulates inactivation kinetics (Lewis and Grandl, 2020) and may interact with the ectodomain of the cadherin protein superfamily (Wang et al., 2022). Knockdown of E-cadherin via siRNA decreases mechanically induced ionic currents in an immortalized cell model of Piezo1 currents (Wang et al., 2022). Co-transfection of Piezo2 with E-cadherin in immortalized cell models increases mechanical currents without affecting inactivation kinetics (Wang et al., 2022), but this interaction is not known outside of cultured cell models.

In epithelial cells, cadherins are integral membrane proteins that mediate physical cell–cell adhesion. E-cadherin is expressed by epithelial cells, where it localizes to the lateral plasma membrane and mediates adherens-type junctions between epithelial cells (Lecuit and Yap, 2015). E-cadherin is part of a mechanosensory complex on the epithelial cells' lateral wall that includes scaffold proteins to anchor intracellularly to the actin cytoskeleton (Lecuit and Yap, 2015). The catenin family of molecules binds to the intracellular tail of E-cadherin (Ozawa et al., 1989; Reynolds et al., 1994), from where it can stabilize E-cadherin (Ireton et al., 2002; Davis et al., 2003), regulate cytoskeletal reorganization (Noren et al., 2000), and facilitate force-dependent tethering to the actin cytoskeleton. The E-cadherin–β/γ-catenin–α-catenin–actin filament chain tethers E-cadherin to the actin cytoskeleton (Sako et al, 1998). Vinculin is a filamentous actin-binding protein that is recruited after tension unfolds the α-catenin molecule (Choi et al., 2012; Yao et al., 2014).

In this study, we hypothesized that Piezo2 interactions with E-cadherin are important for mechanosensation in GI EECs. To test this hypothesis, we set out to visualize Piezo2 co-localization with E-cadherin and assay functional activity in specialized GI epithelial mechanoreceptors, the EECs.

Materials and methods

Ethical approval

All experimental procedures were approved by the Institutional Animal Care and Use Committee (IACUC) of the Mayo Clinic.

Materials

All materials used for experiments, including antibodies employed in immunofluorescence and co-immunoprecipitation studies, are listed in Table 1.

Animals

NeuroD1-Cre mice were a kind gift of Dr. Andrew Leiter (University of Massachusetts, Worcester, MA, USA, since then submitted to The Jackson Laboratories: Jax 028364). Piezo2-Cre and Piezo2$^{f/f}$ mice were kind gifts of Dr. Ardem Patapoutian (Scripps Research Institute, San Diego, CA, USA, since then submitted to The Jackson Laboratories: Jax 027719, 027720). Mouse lines obtained from The Jackson Laboratories: wild type C57BL/6J (Jax 000664), Polr2aTn(pb-CAG-GCaMP5g,-tdTomato)Tvrd/J (Jax 024477), and B6.Cg-Tg(Vil1-cre)1000Gum/J (Jax 021504). Mice were housed in an institutional facility with ad libitum access to food and water. Mice were sacrificed according to ethical guidelines using a fatal dose of rising levels of carbon dioxide. Cervical dislocation served as a secondary measure of euthanasia.

Primary intestinal epithelial cell dissociation

Primary murine colon cultures were prepared from wild type mice sacrificed at 7 wk based on published culture methods (Alcaino et al., 2018; Treichel et al., 2022). Dissociations were made from colonic epithelia because these are more resilient than their intestinal counterparts and more likely to survive for experimentation. The 10-cm segment of colon was removed and placed in ice-cold phosphate-buffered saline (PBS). A blunt tip syringe was used to flush the colon of fecal matter. Small spring scissors were used to remove any mesentery remaining on the colon. After cleaning, isolation of the submucosa and mucosal layers was done by peeling the outer muscle layers with fine forceps. The remaining mucosa and submucosa were minced until the tissue mass resembled a liquid and subsequently washed three times with fresh ice-cold PBS. Tissue was digested in a prewarmed digestion medium consisting of 500 ml DMEM (Sigma-Aldrich), 500 mg BSA (Sigma-Aldrich), 24 mg collagenase XI (Sigma-Aldrich), and 1 ml of PBS. Tissue was digested in four cycles of varying durations: the first cycle was 5 min, second was 10 min, third was 10 min, and fourth was 15 min. At each digestion, this media-cell solution was shaken vigorously to ensure dissociation into single cells, followed by centrifugation. Supernatants from the first two digestions were discarded. Supernatants from the last two digestions were collected and spun at 100 × *g* for 5 min. The resulting pellet was resuspended in culture media, which consisted of 500 ml DMEM (Sigma-Aldrich), 25 ml FBS, HI (Sigma-Aldrich), 5 ml L-glutamine (Life Technologies), and 5 ml Pen/Strep (Sigma-Aldrich).

Organoid preparation

Organoids were generated from four distinct wild type mice. Small intestine organoids were generated, as previously described (Alcaino et al., 2018), to increase our likelihood of consistently identifying EECs making cell–cell contacts with surrounding epithelia. Wild type mice were sacrificed as indicated above. The small bowel was removed from the abdominal cavity. After opening the small bowel longitudinally, it was cut into small sections and washed 15 times with calcium- and magnesium-free Dulbecco's PBS (DPBS; StemCell Technologies). Washed segments were dissociated with Gentle Cell Dissociation Reagent (GCDR; StemCell Technologies) for 15 min and filtered

Table 1. **Table of reagents**

Reagent	Vendor	Catalog no.
Mice		
Wild-type C57BL/6J	Jackson Laboratories	Jax 000664
NeuroD1-Cre (gift from Leiter lab, UMass)	Jackson Laboratories	Jax 028364
TdTomato-GcaMP	Jackson Laboratories	Jax 024477
Villin1-Cre	Jackson Laboratories	Jax 021504
Piezo2-Cre (gift from Patapoutian lab, Scripps Research)	Jackson Laboratories	Jax 027719
Piezo2$^{f/f}$ (gift from Patapoutian lab, Scripps Research)	Jackson Laboratories	Jax 027720
Primers		
Villin forward primer: 5′-TCA AAGGCTCTCTCAC-3′	Origene	MP218222
Villin reverse primer: 5′-AGC AGTCACCATCGAAGAAGC-3′	Origene	MP218222
Piezo2 forward primer: 5′-GCACTCTACCTCAGGAAGACT G-3′	Origene	MP214282
Piezo2 reverse primer: 5′-CAAAGCTGTGCCACCAGGTTC T-3′	Origene	MP214282
Chromogranin A forward primer: 5′-AGAACCAGAGCC CTGATGCCAA-3′	Origene	MP202538
Chromogranin A reverse primer: 5′-CTCTGTGGTTGC CTCAAAGCCA-3′	Origene	MP202538
β-actin forward primer: 5′-GGCTGTATTCCCCTCCATCG-3′	IDT	
β-actin reverse primer: 5′-CCAGTTGGTAACAATGCCATG T-3′	IDT	
HPRT forward primer: 5′-TGG ATACAGGCCAGACTTTGTT-3′	Origene	MP206455
HPRT reverse primer: 5′-CAG ATTCAACTTGCGCTCATC-3′	Origene	MP206455
Antibodies		
Rabbit Piezo2 antibody (IF)	Novus Biologicals	NBP1-78624
Goat 5-HT antibody (IF)	Abcam	ab66047 *validated in PMID: 32407674*
Goat E-cadherin antibody (IF)	Biotechne	AF748 *validated in PMID: 37225711*
Rabbit IgG isotype control	Novus Biologicals	NBP2-24891
Goat IgG isotype control	Abcam	ab37373
Donkey anti-Goat IgG (H&L) FITC	Jackson ImmunoResearch	705-096-147

Table 1. **Table of reagents (*Continued*)**

Reagent	Vendor	Catalog no.
Donkey anti-Rabbit IgG (H&L) Cy5	Jackson ImmunoResearch	711-175-152
Rabbit Piezo2 antibody (co-IP protein detection)	Novus Biologicals	NBP2-61130
Rabbit E-cadherin antibody (co-IP protein detection)	Cell Signaling Technology	3195
Normal rabbit IgG	Cell Signaling Technology	2729
Rabbit catenin δ-1 antibody (co-IP protein detection)	Cell Signaling Technology	59854
Rabbit β-catenin antibody (co-IP protein detection)	Cell Signaling Technology	8480
Rabbit γ-catenin antibody (co-IP protein detection)	Cell Signaling Technology	2309
Rabbit α-catenin antibody (co-IP protein detection)	Cell Signaling Technology	3236
Rabbit vinculin antibody (co-IP protein detection)	Cell Signaling Technology	13901
Rabbit Pan-actin antibody (co-IP protein detection)	Cell Signaling Technology	8465
Others (chemicals, media, materials, etc.)		
Capturem IP & Co-IP Kit	Takara Bio	635721
12–230 kDa separation module	Thermo Fisher Scientific	NC1461323
66–440 kDa separation module	Thermo Fisher Scientific	NC1247135
ProteinSimple anti-rabbit detection module	Thermo Fisher Scientific	NC1196891
35-mm glass bottom dishes	MatTek Corporation	P35G-1.5-14-C
Matrigel GFR and Phenol red free basement membrane matrix	Corning	356231
Dulbecco's modified eagle's medium	Sigma-Aldrich	D6429
Bovine serum albumin	Sigma-Aldrich	A7906
Collagenase Type XI	Sigma-Aldrich	C9407
Fetal bovine serum	Thermo Fisher Scientific	35-011-CV
Penicillin/streptomycin	Thermo Fisher Scientific	221674
L-glutamine	Thermo Fisher Scientific	25030081
Gentle cell dissociation reagent	StemCell Technologies	7174
IntestiCult organoid growth medium (Mouse)	StemCell Technologies	06005
Dulbecco's phosphate-buffered saline (Ca^{++}, Mg^{++} free)	StemCell Technologies	37354
Accell mouse non-target siRNA	Horizon (PerkinElmer)	D-001910

Table 1. **Table of reagents (*Continued*)**

Reagent	Vendor	Catalog no.
Accell mouse Piezo2 siRNA	Horizon (PerkinElmer)	E-163012
Accell mouse E-cadherin siRNA	Horizon (PerkinElmer)	E-041028
Phalloidin Atto 565	Sigma-Aldrich	94072
OCT embedding compound	Sakura Finetek	4583
UltraCruz blocking reagent	Santa Cruz Biotechnology	516214

with a 70 µm cell strainer. The filtered suspension was centrifuged at 500 × *g* and 4°C for 5–10 min and resuspended in DMEM (ATCC). After another centrifugation step under the same conditions, the pelleted crypts were resuspended in IntestiCult Organoid Growth Medium (IOGM, StemCell Technologies) and mixed at a 1:1 ratio with Matrigel (Corning). 400 µl domes were plated in prewarmed 6-well dishes (Corning) and cultured in 3 ml IOGM per well.

Tissue super-resolution imaging and immunohistochemistry

Flat sheets (1 cm × 0.5 cm) of small bowel were used. Tissues were fixed in 4% PFA-PB for 4 h separately, washed in PBS, and moved into 30% sucrose in PBS until they were frozen in an OCT embedding compound (Sakura Finetek). Tissues were cut into 12-µm-thick sections, rinsed with PBS twice for 5 min, and blocked with 200 µl per slide of 1% BSA/PBS/0.3% Triton X/10% normal donkey serum in a humidity chamber. Primary antibodies were added in 200 µl per slide of BSA/PBS/0.3% Triton/10% normal donkey serum and were incubated at 4°C overnight in a humidity chamber. Slides were then rinsed five times for 3 min in PBS. The secondary antibody was incubated for 1 h in the dark. Slides were mounted in SlowFade gold with DAPI (Life Technologies) mounting buffer.

An Elyra PS.1 Super Resolution microscope (Carl Zeiss Microscopy, LLC) with a 63×, 1.4 NA oil-immersion objective and a 1.5× tube multiplier was used. Laser-excitation wavelengths were 405, 488, 561, and 642 nm. The z-sections ranged from 8 to 10 µm, with a slice thickness of 175 nm. A four-image average was used for each z-slice of each of the five rotations of the grid. Channels were acquired sequentially, beginning with the 642-nm excitation, and ending with 405 nm. ZEN deconvolution software for SIM was used with default settings.

Organoid super-resolution imaging and whole-mount organoid immunofluorescence

Organoids were grown in 50% Matrigel domes for 1-wk after passage. Organoid domes were washed with PBS and fixed in 4% PFA for 30 min at room temperature. Subsequently, they were permeabilized with 0.3% Triton X-100 (Thermo Fisher Scientific), blocked with UltraCruz Blocking Reagent (Santa Cruz), and incubated with primary antibodies overnight at 4°C. On the next day, they were washed with PBS, incubated with secondary antibodies for 1 h at room temperature, and mounted.

An LSM 980 microscope with Airyscan 2 (Carl Zeiss Microscopy, LLC) was used for super-resolution imaging with a 63×, 1.4 NA oil immersion objective. Excitation wavelengths: 353, 493, 577, and 653 nm. Airyscan modality was used during imaging, and default ZEN reconstruction settings were used for creating the super-resolution images.

Fluorescence profiles and co-localization measurements

Fluorescence profiles were generated with Zen blue software (Zeiss) and normalized with respect to maxima and minima in the traces. Manders' correlation coefficients (MCCs) were generated using the JACoP plug-in in ImageJ (Bolte and Cordelières, 2006; Schneider et al., 2012) from inset images of each of the subcellular domains. Thresholds were applied consistently across analyses. Statistical analyses were performed with Prism 9 (GraphPad).

RNA isolation and qRT-PCR analysis

Total mRNA was isolated from vil^{Cre}xPiezo2$^{f/f}$ and Piezo2$^{f/f}$ organoids using the RNeasy micro kit (Qiagen). cDNA was synthesized with SuperScript VILO (Thermo Fisher Scientific). Quantitative real-time polymerase chain reaction (qRT-PCR) was performed using FastStart Essential DNA Green Master (Roche Diagnostics) and analyzed using a LightCycler 96 (Roche Diagnostics). qRT-PCR primers used in this study (Integrated DNA Technologies) are listed in Table 1.

Co-immunoprecipitation and protein immunoassay

Colon epithelial cell suspensions from six mice were lysed and immunoprecipitated using the Capturem Co-IP kit (Takara Bio) following the manufacturer's instructions. Samples were centrifuged at 17,000 × *g* and 4°C for 10 min. The supernatants were divided into five fractions: (1) input fraction, (2) no antibody control fraction, (3) rabbit IgG control fraction, (4) Piezo2 immunoprecipitation fraction, and (5) E-cadherin immunoprecipitation fraction. The number of fractions generated from a single mouse suspension depended on the yield from the primary dissociation. At least three biological replicates were generated for each fraction. Fraction 1 was immediately saved for blotting. Fraction 2 was not incubated with any antibody. Fractions 3–5 were incubated for 20 min at room temperature with a rabbit IgG control antibody or validated antibodies against specified targets at a 1:300 dilution, respectively. The binding of the immunoprecipitate to the column, washing, and elution were carried out for fractions 2–5 exactly to the manufacturer's instructions using the provided solutions and a tabletop centrifuge. We used a colorimetric Bradford reaction (Bio-Rad) to determine the overall protein concentration in each of the samples using known concentrations of bovine serum albumin (BSA) to build a standard curve. We used the colorimetric reaction to consistently load the same amount of protein per experiment. We loaded 500 ng of protein in all wells for protein detection.

Protein detection was performed via Simple Western in a capillary-based automated instrument that carries out the electrophoretic separation of proteins and their immunodetection in tandem reactions (Jess, ProteinSimple). Samples were diluted

with wash buffer and reconstituted with the manufacturer's 10X sample buffer and 5X master mix for protein detection. We utilized two of the manufacturer's detection modules for different proteins: 12–230 kDa module for the detection of δ-1 catenin, β-catenin, γ-catenin, α-catenin, vinculin, and actin; 66–440 kDa module for the detection of Piezo2 and E-cadherin. A chemiluminescence assay was selected. We used the manufacturer's anti-rabbit detection module, which includes a conjugated anti-rabbit secondary antibody, for detection. Assay plates were loaded with 500 ng of protein per sample, biotinylated ladder, primary antibodies, blocking solution, secondary antibody, and luminol-peroxide substrate following the manufacturer's instructions. Blot-equivalent images, electropherogram profiles, and protein peak areas for quantification were acquired from the Compass for Simple Western software (ProteinSimple).

Calcium imaging

Calcium imaging protocols are like those previously published (Alcaino et al., 2018; Treichel et al., 2022; Knutson et al., 2022). Dissociated single cells were imaged on an inverted Olympus IX70 epifluorescence microscope equipped with a 16-bit high-speed camera (ORCA-Flash4.0; Hamamatsu) and a CoolLED pE-300Ultra illumination system (CoolLED Limited). pCLAMP10.6 (Molecular Devices) was used to drive a piezotransducer microindenter, LED illumination system, Hamamatsu camera, and Metamorph imaging software (Molecular Devices). The bath solution contained: 127 mM NaCl, 3 mM KCl, 1 mM $MgCl_2$, 2.5 mM $CaCl_2$, 10 mM glucose, and 10 mM Hepes, pH 7.3, 320 mmol/kg (adjusted with sucrose). EECs were identified by tdTomato fluorescence (excitation/emission 554/581 nm) and studied functionally using GCaMP5 (excitation/emission 480–505/525 nm). Where noted, dissociated primary cells from three mice were randomly assigned to be transfected with 20 nM of Accell Mouse E-cadherin siRNA SMARTpool (E–041028-00-0005; Dharmacon), or 20 nM of Accell Non-Target control siRNA (D-001910-10-05; Dharmacon). Both cohorts (NT siRNA treated, E-cadherin siRNA-treated) contained cells from the three mice. Experiments were performed 48–72 h after the addition of siRNA-supplemented media.

For mechanical stimulation, a 0.8-µm indentation was delivered for 50 ms with a fire-polished glass microcapillary driven by a piezotransducer P-621.1CD attached to an E-625.CR controller (Physik Instrumente). Raw fluorescence from GcaMP5+ cells was exported to Microsoft Excel and converted to $\Delta F/F_0$ [$\Delta F/F_0 = (F - F_0)/F_0$], where F_0 is the baseline fluorescence immediately before stimulation. Peak $\Delta F/F_0$ values were extracted from the $\Delta F/F_0$ traces. Areas under the curve (AUCs) were calculated from $\Delta F/F_0$ traces. Statistical analyses were performed with Prism 9 (GraphPad).

Online supplemental material

Fig. S1 contains additional immunofluorescence imaging of Piezo2 in GI epithelia. Fig. S2 demonstrates our validation of the immunofluorescence approaches, including the Piezo2 antibody used for labeling. Fig. S3 contains additional immunofluorescence imaging of Piezo2 and E-cadherin in intestinal organoids; these images were used to generate average MCCs in Fig. 2. Fig. S4 shows inverse MCCs to those shown in Fig. 2. Fig. S5 contains uncropped versions of the protein immunoassays in Fig. 2. Fig. S6 validates the E-cadherin knockdown approach via immunofluorescence.

Results

Piezo2 localizes to the lateral plasma membrane of GI EC cells in vivo and in an organoid model of GI epithelia

Piezo2 is expressed in multiple cellular compartments of mechanosensitive EC cells (Alcaino et al., 2018). We used super-resolution imaging of GI tissues and organoids to examine the subcellular distribution of the ion channel (Fig. 1 A). EC cells were 5-HT immunoreactive using a validated antibody (Beumer et al., 2020). A subpopulation of these 5-HT-positive cells was also positive for Piezo2 in tissues and organoids of all probed mice (three mice used for tissues, four for organoid generation) (Fig. 1, B and E; and Fig. S1). F-actin staining allowed us to discern the cellular borders since F-actin accumulation in the microvilli and the apical plate resulted in a significantly brighter signal toward the apical compartment, and the cortical actin network allowed us to discern the rest of the cell outlines (Fig. 1, B and E; Fig. S1; Fig. S2; and Fig. S3). We corroborated the Piezo2 antibody sensitivity and specificity via immunofluorescent labeling of organoids derived from Piezo2-Cre::GcaMP5/tdTomato and villin-Cre::$Piezo2^{f/f}$ mice (Fig. S2, A–C). Control immunofluorescence experiments using isotype controls or lacking primary antibodies confirmed the specificity of these results (Fig. S2, D–G).

We noted Piezo2 distributed to three locations in primary EC cells: (1) overlapping with F-actin at the lateral wall (LW) (Fig. 1, B and C denoted by ‡), (2) in basal cytoplasmic (BC) accumulations (Fig. 1, B and C, denoted by ¶), and (3) in the perinuclear (Pn) cytoplasm (Fig. 1, B and C, denoted by §). Surprisingly, we rarely observed the Piezo2 signal in the apical EC cell compartment. We observed the same subcellar distributions in organoid 5-HT+/Piezo2+ double-positive cells (Fig. 1, E and F). Piezo2 and actin fluorescence profiles in both tissue and organoids demonstrated substantial F-actin accumulation with Piezo2 at the LW (Fig. 1, D and G). Profiles did not show as strong a correlation between Piezo2 and actin in the two other domains where the channel localizes (Fig. 1, D and G).

E-cadherin co-localizes with Piezo2 in an organoid model of GI epithelia

Piezo2 distribution was consistent between organoids and tissues, and since intestinal organoids provide a readily accessible three-dimensional model with spontaneously differentiated EECs, we pursued further imaging in organoids. We sought to establish co-localization between Piezo2 and E-cadherin since the two molecules have been reported to interact in cellular overexpression systems (Wang et al., 2022). We noted the same three pools of subcellular Piezo2 (Fig. 2 A, symbols consistent with Fig. 1 and Fig. S3). As expected, E-cadherin immunofluorescence using a validated antibody (Alvizi et al., 2023) localized mostly to the basolateral aspects of all epithelial cells in the

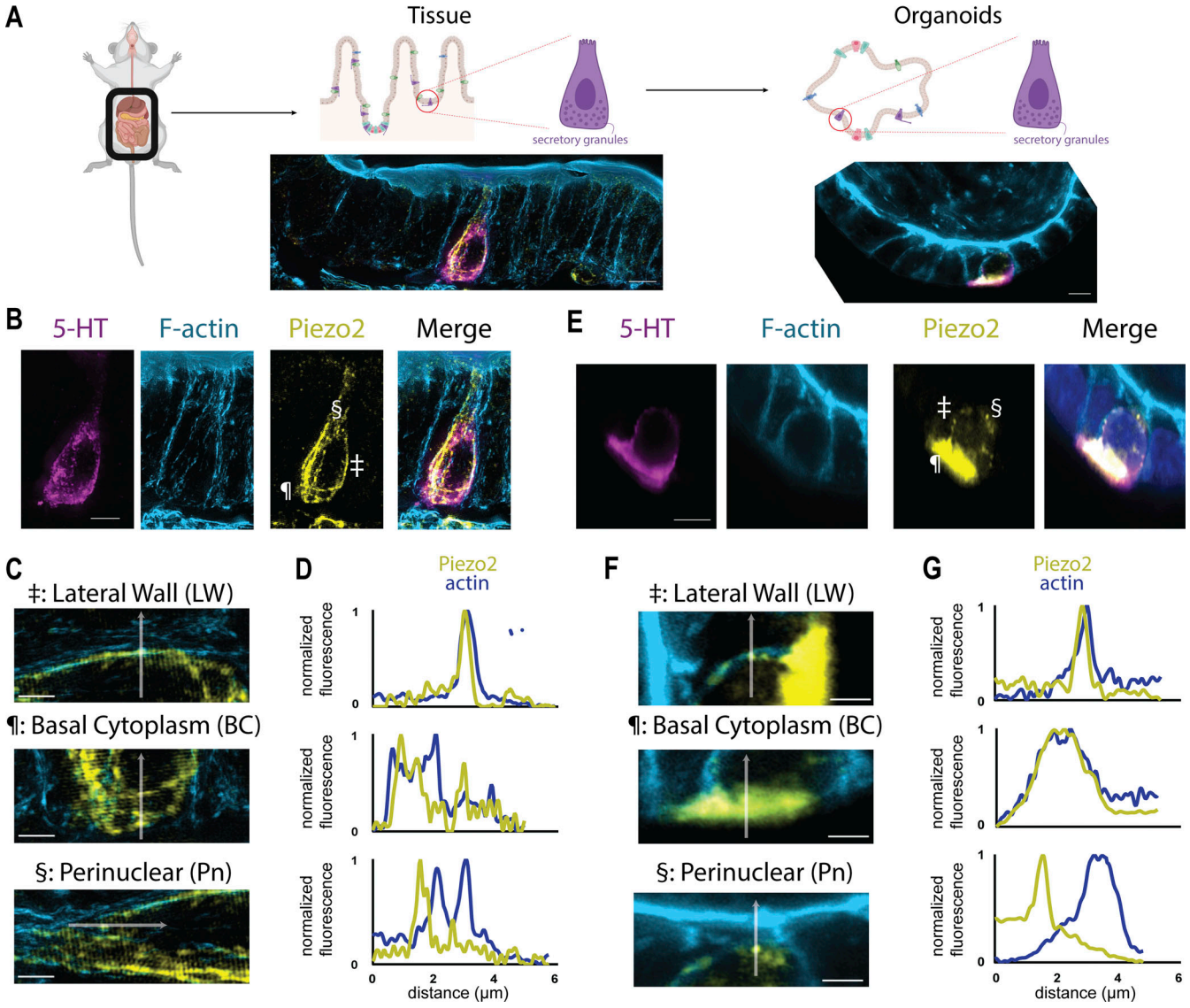

Figure 1. **Piezo2 subcellular localization in intestinal epithelial mechanoreceptors. (A, B, and E)** Serotonin (5-HT)-secreting enterochromaffin (EC) cells were identified in tissues and organoids by virtue of 5-HT immunofluorescence (B and E, first panel). Cell borders were defined by F-actin labeling (B and E, second panel). **(C and F)** Super-resolution labeling of Piezo2 ion channel clusters shows three patterns of distribution in tissue (C) and organoids (F). **(D and G)** Areas marked with ‡ in B and E correspond to Piezo2 that localizes to the lateral cell wall, where it overlaps with F-actin labeling by fluorescence profile (D and G). Areas marked with ¶ in B and E correspond to Piezo2 that localizes to the basal cytoplasm, where it weakly overlaps with F-actin labeling by fluorescence profile (D and G). Areas marked with § correspond to a perinuclear pattern of Piezo2 distribution. This pool does not appear to overlap with F-actin labeling by fluorescence profile (D and G). Fluorescence profiles in D and G correspond to the arrow in the images immediately to their left. Profiles are normalized to the average fluorescence intensity across the whole cell. Scale bars: 5 µm (A, B, and E), 2 µm (C and F). Diagrams in panel A created with Biorender.

organoid model (Fig. 2, A and C; and Fig. S3). E-cadherin is expected to mediate Piezo2 tethering to the actin cytoskeleton, and since previous fluorescence profiles showed strongest association between Piezo2 and F-actin accumulation at the LW (Fig. 1, D and G), we first fixated on the LW. Fluorescence profiles showed that part of the E-cadherin signal increased at the LW along with Piezo2 (Fig. 2 B and Fig. S3). The correlation between Piezo2 and E-cadherin fluorescence signals was more pronounced at the LW and the basal cytoplasm than in the perinuclear region (Fig. 2, C and D). To quantify these associations, we calculated MCCs of Piezo2 over F-actin and E-cadherin (Fig. 2 E and Fig. S3). Calculating MCCs over the whole cell (WC) revealed that ∼30% of the entire Piezo2 immunofluorescent signal overlapped with F-actin staining. Conversely, two-thirds of the entire Piezo2 immunofluorescent signal overlapped with that of E-cadherin in the WC. When analyzed by subcellular pools, an average of 72% of the Piezo2 signal overlapped with that of F-actin at the LW, whereas the correlation was more modest in the basal cytoplasm (23% on average across all analyzed cells). We consistently found very little overlap between Piezo2 and F-actin in the perinuclear region. The overlap between Piezo2 and E-cadherin was also strongest at the LW (average 78%, very close to the Piezo2/F-actin average). We additionally noted significant Piezo2/E-cadherin overlap in the basal cytoplasm

(average 66% across all analyzed cells). As with F-actin, the Piezo2/E-cadherin overlap was consistently nearly absent in the perinuclear region. As expected, the F-actin/Piezo2 and E-cadherin/Piezo2 MCCs were lower for the WC and across all subcellular locations (Fig. S4).

E-cadherin and actin interact with Piezo2 in primary GI epithelia

Since the majority of Piezo2 signals at the LW co-localized with that of E-cadherin and actin, we sought to confirm that these molecules interact with each other. We also asked whether the adaptor proteins that link E-cadherin to the actin cytoskeleton were part of the proposed Piezo2–E-cadherin complex in EECs. Mucosal Piezo2 expression is largely restricted to EECs (Alcaino et al., 2018; Billing et al., 2019; Treichel et al., 2022). Hence, we performed co-immunoprecipitation experiments using stripped mucosal segments, which consist mostly of epithelial cells. We immunoprecipitated Piezo2 or E-cadherin and used a high-sensitivity protein separation and immunodetection assay to probe the molecules that co-immunoprecipitated with either protein. E-cadherin co-immunoprecipitated Piezo2, and, as expected, also co-immunoprecipitated actin and the associated proteins catenin δ-1 (p120 catenin), β-catenin, γ-catenin, α-catenin, and vinculin (Fig. 2, F and G). In the Piezo2 precipitates, we co-immunoprecipitated E-cadherin and actin, along with catenin δ-1 (p120 catenin), γ-catenin, α-catenin, and vinculin (Fig. 2, F and G). Protein band quantification confirmed protein accumulation in the precipitates over the column and antibody controls (Fig. 2 G and Fig. S5).

E-cadherin knockdown decreases calcium responses to mechanical stimuli in EECs

Since Piezo2 interacts with E-cadherin in GI EECs, we next asked whether this interaction has a functional relevance in EEC mechanosensitivity. To answer this, we dissociated epithelia from NeuroD1-Cre::GCaMP5/tdTomato mice, where the genetically encoded calcium indicator GCaMP5 is expressed by cells expressing NeuroD1 (Alcaino et al., 2018; Treichel et al., 2022; Knutson et al., 2022), a late-stage transcription factor defining EEC fate (Haber et al., 2017). Dissociated cells were cultured in the presence of either non-targeting (NT) or E-cadherin siRNA for at least 48 h. Immunofluorescence showed no apparent difference in the expression or distribution of Piezo2 while confirming decreased E-cadherin protein levels (Fig. S6). To test the function, we mechanically stimulated via a single 50-ms blunt indentation (Fig. 3 A). Individual EECs were identified by tdTomato fluorescence (Fig. 3 B), and acute intracellular calcium (Ca^{2+}) activity was measured by GCaMP5 fluorescence (Fig. 3, C and D). A proportion of NT siRNA-treated cells (11/16) showed the characteristic mechanosensitive Ca^{2+} response we had previously observed in mechanosensitive EECs and which we had previously proven to be Piezo2-dependent (Alcaino et al., 2018) (Fig. 3 C). E-cadherin knockdown diminished the peak calcium response to mechanical stimulation (Fig. 3, C–E) by 64.9 ± 23.1% and AUCs by 68.5 ± 32.6% (Fig. 3, F and G).

Discussion

GI EECs are epithelial mechanoreceptors that require Piezo2 to coordinate GI motility and secretion (Alcaino et al., 2018; Treichel et al., 2022). Piezo2 was suggested to interact with E-cadherin in cultured cell models (Wang et al., 2022). Here, we tested whether Piezo2 interacted with E-cadherin in mechanoreceptors of the GI epithelial lining—mechanosensitive EECs. We also demonstrate this interaction could play a functional role in EEC mechanosensitivity. To our knowledge, this is the first demonstration of interactions between Piezo2 and E-cadherin/actin in primary tissues and organoids.

Intracellularly, E-cadherin anchors to the actin cytoskeleton (Lecuit and Yap, 2015). Our co-immunoprecipitation experiments show that E-cadherin, actin, and the linking proteins that span the two co-immunoprecipitate with Piezo2. As others have shown that Piezo2 ionic currents decrease upon actin depolymerization (Eijkelkamp et al., 2013; Jia et al., 2016; Verkest et al., 2022), here, we report that E-cadherin disruption decreases mechanosensitive Ca^{2+} responses. Piezo2 is a multimodal force sensor that detects both membrane deflection (force-from-lipid) and force transmitted along actin tethers (force-from-filament) (Cox et al., 2019; Verkest et al., 2022; Zhou et al., 2023). Several actin-binding proteins that co-immunoprecipitate with Piezo2—specifically α-catenin and vinculin—are mechanosensitive (le Duc et al., 2010; Twiss et al., 2012; Yao et al., 2014; Noordstra et al., 2023). It is possible that force transmission and Piezo2 activation through force-from-filament may be different than through force-from-lipid, resulting in different responses, especially when the Piezo2+ EECs are integrated back into epithelial monolayers. We conclude that force-from-filament transmission requires a particular focus on the EEC LW since this is the cell domain where we found the strongest overlap between Piezo2, E-cadherin, and F-actin. Of note, neither the Piezo2/F-actin nor the Piezo2/E-cadherin MCCs were perfect ones at the LW and displayed some degree of variability. This suggests that while the vast majority (approximately three-quarters) of Piezo2 clusters tether via E-cadherin at the LW, a fraction of Piezo2 molecules in this domain rely on either lipid-based mechanosensing or on an alternative tether.

Alternatively, the interaction between Piezo2 and E-cadherin/actin may localize Piezo2 to areas of sharp force gradients to optimize cellular mechanosensitivity, such as it has been suggested between VE-cadherin and Piezo1 in endothelial cells (Chuntharpursat-Bon et al., 2019, *Preprint*). Mechanosensitive binding partners such as vinculin might play role in detecting such high-load areas within the cell. Further, the actin cytoskeleton forms "corrals" that compartmentalize regions of the plasma membrane and proteins contained therein (Sadegh et al., 2017), including ion channels (Tamkun et al., 2007). In the EEC, cytoskeletal elements may define mechanical domains for force transduction at the plasma membrane. Channel clustering could extend beyond Piezo2 and include other channels potentially involved in mechanotransduction, similar to how voltage-gated ion channels are clustered in neurons by cytoskeletal domains (Xu et al., 2013; Solé and Tamkun, 2020). Future studies in multicellular cell systems may investigate if E-cadherin and associated structural elements play a role in Piezo2 targeting to,

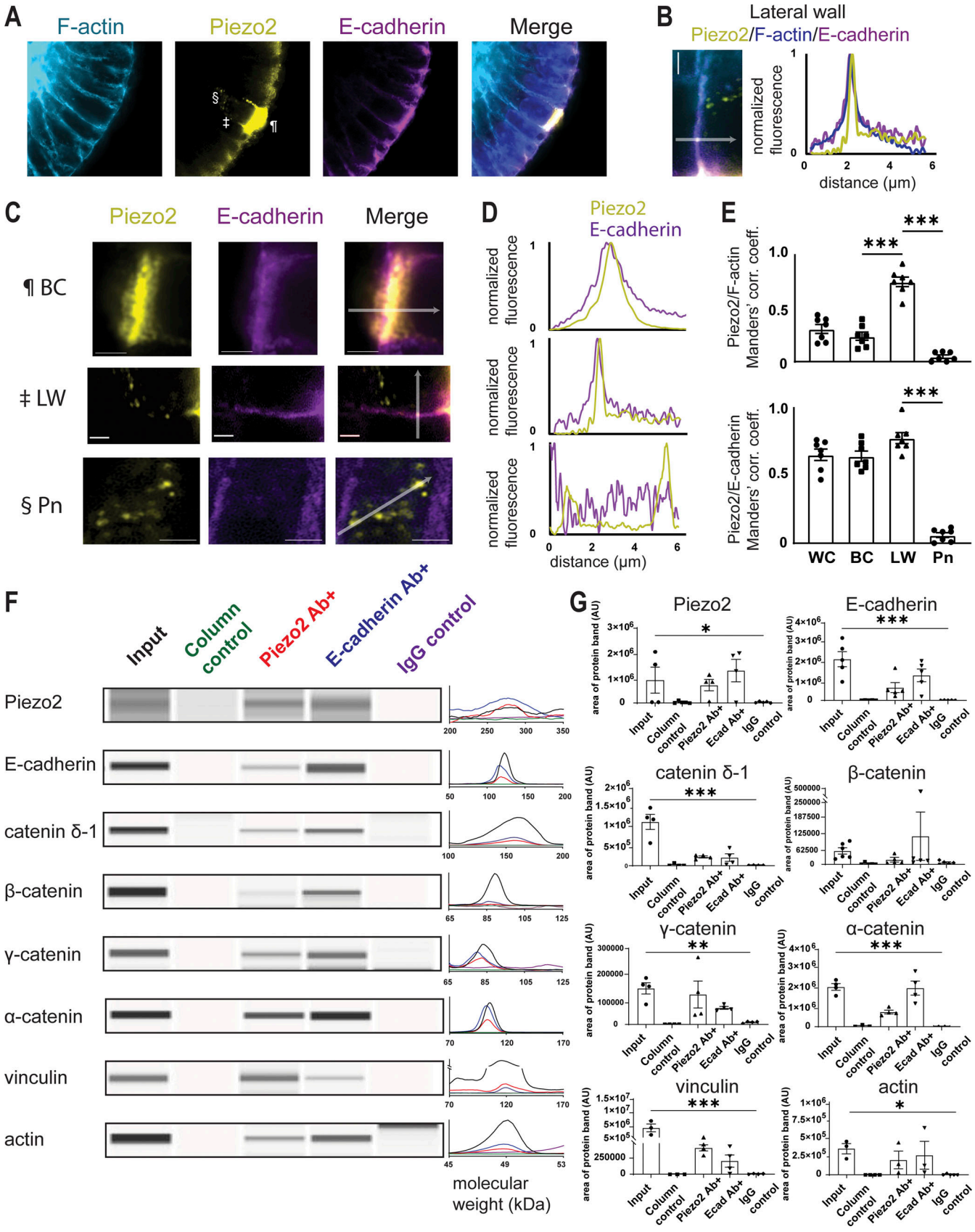

Figure 2. **E-cadherin, actin, and catenin proteins interact with Piezo2 in an organoid model of intestinal epithelia. (A)** Piezo2-expressing mechanoreceptors in an intestinal organoid form cell contacts with surrounding epithelia via E-cadherin. Symbols on the Piezo2 panel (‡, ¶, and §) correspond to those used in Fig. 1 to identify the subcellular domains where we observed Piezo2 signal. **(B)** The lateral wall shows a close association of the three proteins Piezo2,

E-cadherin, and F-actin as shown by their fluorescence profiles. **(C)** Two out of the three subcellular pools of Piezo2 show association with E-cadherin. Piezo2 at the lateral wall (LW) and basal cytoplasm (BC) show partial overlap with E-cadherin. There is no overlap between Piezo2 and E-cadherin in the perinuclear (Pn) space. Profiles in B and D are normalized to the average fluorescence intensity across the whole cell. **(E)** Overlap between Piezo2 and F-actin or E-cadherin was quantified via Manders' correlation coefficients (MCCs). The other images used to generate the data in panel E can be found in Fig. S2. Piezo2/F-actin MCC: whole cell (WC) 0.29 ± 0.04, BC 0.23 ± 0.04, LW 0.72 ± 0.04, Pn 0.04 ± 0.02, P < 0.0001 by one-way ANOVA. Piezo2/E-cadherin MCC: whole cell (WC) 0.66 ± 0.04, BC 0.66 ± 0.04, LW 0.78 ± 0.04, Pn 0.06 ± 0.02, P < 0.0001 by one-way ANOVA. Individual groups were compared via Tukey post-hoc test. **(F)** Piezo2 co-immunoprecipitation from stripped mouse mucosa. Probed protein in each row listed on the left. The input lane consists of the full mucosal lysate. Column control samples were not incubated with any antibody. Piezo2 Ab+ lane was incubated with rabbit anti-Piezo2 antibody. E-cadherin Ab+ lane was incubated with rabbit anti-E-cadherin antibody. IgG control lane was incubated with rabbit IgG antibody. Electropherograms to the right of computer-generated protein bands show protein intensities at the displayed molecular weights. Line profile colors correspond to column sample designations. **(G)** Quantification of protein areas generated by electropherograms in panel F. Each point in a column represents a different mouse. Groups were compared via one-way ANOVA. Fluorescence profiles in B and C correspond to the line profile along the faint white bar in the images immediately to their left. Scale bars: 5 µm (A), 2 µm (B and C). *P < 0.05, **P < 0.01, ***P < 0.001.

and clustering at, the LW. Our combination of immunofluorescence and co-immunoprecipitation in tissues and organoids support the conclusion that a pool of Piezo2 molecules in GI EECs localizes to the lateral membrane, where they interact with E-cadherin and actin. We report that part of the cytoplasmic pool of Piezo2 at the base of the EEC also co-localizes with E-cadherin, though it does not co-localize as strongly with F-actin. These preliminary clues provide testable hypotheses about the temporal sequence of Piezo2–E-cadherin association and tethering to the actin cytoskeleton. The temporal assembly of E-cadherin junctional complexes has been investigated and suggested to include both early associations and late interactions at the cell junction (Bryant and Stow, 2004; Miranda et al., 2003). Piezo2 and E-cadherin may be stored in intracellular vesicles separate from serotonin-containing vesicles, ready for shuttling to the plasma membrane (Alcaino et al., 2018). If so, the Piezo2–E-cadherin interaction may take place prior to Piezo2 localization to the membrane. This potential interpretation would be consistent with the proposed model of Piezo2–E-cadherin interaction, whereby the junctional protein impales the ion channel so the ectodomain of

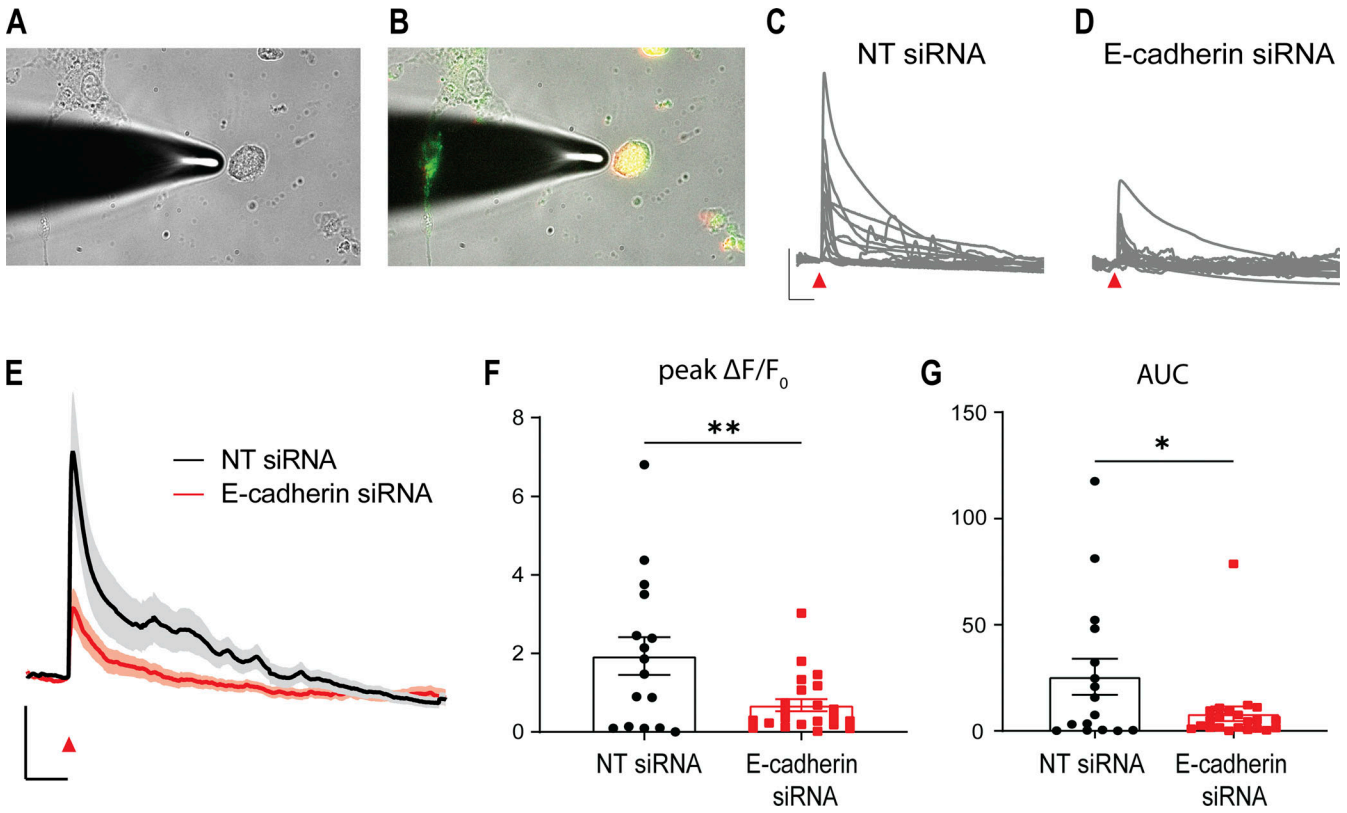

Figure 3. **Piezo2–E-cadherin co-expression is necessary for enteroendocrine mechanosensitivity. (A)** Primary NeuroD1-GCaMP EECs were mechanically stimulated via blunt microindentation. **(B)** EECs were identified by tdTomato/GCaMP double labeling. **(C and D)** Acute fluctuations in GCaMP fluorescence were measured in individual EECs treated with non-target (NT) or E-cadherin-targeting siRNA. Red arrows show the time of mechanical stimulation. Vertical scale bar = 3 $\Delta F/F_0$. Horizontal scale bar = 10 s. **(E)** Average responses created from the individual traces in C and D. Solid lines represent average traces and shaded areas represent SEM. Red arrow shows the time of mechanical stimulation. Vertical scale bar = 1 $\Delta F/F_0$. Horizontal scale bar = 10 s. **(F and G)** Mean ± SEM peak changes in fold-fluorescence (F) and AUCs (G) in the normalized EEC responses in C and D. Circles and squares represent individual cells. Peak fold increase: NT siRNA 1.93 ± 0.48, *n* = 16 cells from three mice; E-cad siRNA 0.68 ± 0.15, *n* = 22 cells from three mice, P = 0.008. AUC: NT siRNA 25.5 ± 8.5, *n* = 16 cells from three mice; E-cad siRNA 8.0 ± 3.7, *n* = 22 cells from three mice, P = 0.043. *P < 0.05, **P < 0.01 via an unpaired two-tailed Student's *t* test.

E-cadherin interacts with the cap domain of Piezo2 (Wang et al., 2022). We did not see interactions between Piezo2 and E-cadherin in the perinuclear pool of Piezo2, perhaps suggesting that actively translated proteins may be too nascent to interact with E-cadherin. However, dedicated experiments that would look at the trafficking of these molecules over time are required to test these hypotheses.

E-cadherin and Piezo2 are co-expressed in several epithelial mechanoreceptors. These include linings in the skin (Woo et al., 2014), lung (Nonomura et al., 2017), and bladder (Marshall et al., 2020), where Piezo2 mechanosensitivity is critical for physiologic function. Yet the interactions between molecular mechanosensors may have implications broader than sensory mechanotransduction. Diseases like cancer display mechanobiological features that impact progression and survival (Rao et al., 2021). While the mechanistic role of Piezo2 in cancer remains to be elucidated, E-cadherin protein expression is still detectable in solid tumors upon Piezo2 overexpression and E-cadherin downregulation (Katsuta et al., 2022). Classically, E-cadherin downregulation is perceived to correlate with more invasive cancer phenotypes as part of the epithelial-to-mesenchymal transition (EMT) (van Roy, 2014). Nevertheless, this is not always the case, as metastases may continue to express E-cadherin, and positive roles for E-cadherin in metastases have been reported (Na et al., 2020). Piezo2 expression correlates with lymph node infiltration in patients with colorectal cancer (Liu et al., 2022). Future experiments will be necessary to discern if E-cadherin similarly persists in colorectal cancer, and if so, whether it is potentiating Piezo2 activity and affecting cancer cell invasiveness. Since the effect of Piezo2 expression in cancer is tissue-dependent (Liu et al., 2022), interactions such as the Piezo2–E-cadherin interaction (and others) may shift the balance between positive and negative outcomes.

In summary, we found that in specialized GI epithelial mechanoreceptors, a fraction of the Piezo2 pool localizes to the lateral membrane, where it interacts with E-cadherin, actin, and other cytoskeletal-binding mechanosensors; and that this interaction may affect Piezo2-mediated cellular mechanosensitivity. It is possible that the Piezo2–E-cadherin interaction is an important anchor for Piezo2 to detect forces transmitted along epithelial tissues, which connect their cytoskeletons into supracellular networks that span across the tissue (Lecuit and Yap, 2015). The connections between Piezo2 and structural proteins, including E-cadherin and actin, have important implications in sensory mechanotransduction and tissue mechanotransduction in health and disease.

Data availability

The data underlying Fig. 2 are available in the supplemental material. Any further data are available from the corresponding author upon request.

Acknowledgments

Jeanne M. Nerbonne served as editor.

The authors thank Drs. Deborah Leckband and Gina Razidlo for constructive intellectual discussions and Mr. Eugene Krueger for assistance with super-resolution imaging and image analysis. We thank Mrs. Lyndsay Busby for administrative support.

This work was supported by the National Institutes of Health (NIH) grants: GM065841, DK128913, DP2AT010875, DK123549, DK052766, TR002379, and DK084567 (Mayo Center for Cell Signaling in Gastroenterology).

Author contributions: A. Mercado-Perez: Conceptualization, Data curation, Formal analysis, Funding acquisition, Investigation, Methodology, Visualization, Writing - original draft, Writing - review & editing, J.P. Hernandez: Investigation, Y. Fedyshyn: Data curation, Methodology, Validation, Writing - review & editing, A.J. Treichel: Investigation, Methodology, V. Joshi: Investigation, Writing - review & editing, K. Kossick: Resources, K.R. Betageri: Formal analysis, Investigation, G. Farrugia: Conceptualization, Methodology, Project administration, Resources, B. Druliner: Investigation, Resources, Supervision, Writing - review & editing, A. Beyder: Conceptualization, Data curation, Formal analysis, Funding acquisition, Investigation, Methodology, Project administration, Resources, Supervision, Validation, Visualization, Writing - original draft, Writing - review & editing.

Disclosures: The authors declare no competing interests exist.

Submitted: 22 December 2022
Revised: 20 January 2024
Revised: 18 May 2024
Revised: 18 August 2024
Accepted: 19 September 2024

References

Alcaino, C., K.R. Knutson, A.J. Treichel, G. Yildiz, P.R. Strege, D.R. Linden, J.H. Li, A.B. Leiter, J.H. Szurszewski, G. Farrugia, and A. Beyder. 2018. A population of gut epithelial enterochromaffin cells is mechanosensitive and requires Piezo2 to convert force into serotonin release. *Proc. Natl. Acad. Sci. USA*. 115:E7632–E7641. https://doi.org/10.1073/pnas.1804938115

Alvizi, L., D. Nani, L.A. Brito, G.S. Kobayashi, M.R. Passos-Bueno, and R. Mayor. 2023. Neural crest E-cadherin loss drives cleft lip/palate by epigenetic modulation via pro-inflammatory gene-environment interaction. *Nat. Commun.* 14:2868. https://doi.org/10.1038/s41467-023-38526-1

Beumer, J., J. Puschhof, J. Bauzá-Martinez, A. Martínez-Silgado, R. Elmentaite, K.R. James, A. Ross, D. Hendriks, B. Artegiani, G.A. Busslinger, et al. 2020. High-resolution mRNA and secretome atlas of human enteroendocrine cells. *Cell*. 181:1291–1306.e19. https://doi.org/10.1016/j.cell.2020.04.036

Beyder, A. 2019. In pursuit of the epithelial mechanosensitivity mechanisms. *Front. Endocrinol. (Lausanne)*. 9:804. https://doi.org/10.3389/fendo.2018.00804

Billing, L.J., P. Larraufie, J. Lewis, A. Leiter, J. Li, B. Lam, G.S. Yeo, D.A. Goldspink, R.G. Kay, F.M. Gribble, and F. Reimann. 2019. Single cell transcriptomic profiling of large intestinal enteroendocrine cells in mice - identification of selective stimuli for insulin-like peptide-5 and glucagon-like peptide-1 co-expressing cells. *Mol. Metab.* 29:158–169. https://doi.org/10.1016/j.molmet.2019.09.001

Bolte, S., and F.P. Cordelières. 2006. A guided tour into subcellular colocalization analysis in light microscopy. *J. Microsc.* 224:213–232. https://doi.org/10.1111/j.1365-2818.2006.01706.x

Bryant, D.M., and J.L. Stow. 2004. The ins and outs of E-cadherin trafficking. *Trends Cell Biol.* 14:427–434. https://doi.org/10.1016/j.tcb.2004.07.007

Bulbring, E., and A. Crema. 1959. The release of 5-hydroxytryptamine in relation to pressure exerted on the intestinal mucosa. *J. Physiol.* 146:18–28. https://doi.org/10.1113/jphysiol.1959.sp006175

Choi, H.J., S. Pokutta, G.W. Cadwell, A.A. Bobkov, L.A. Bankston, R.C. Liddington, and W.I. Weis. 2012. αE-catenin is an autoinhibited molecule that coactivates vinculin. *Proc. Natl. Acad. Sci. USA*. 109:8576–8581. https://doi.org/10.1073/pnas.1203906109

Chuntharpursat-Bon, E., O. Povstyan, M. Ludlow, H. Gaunt, P. Baxter, and D. Beech. 2019. Cell adhesion molecule interaction with Piezo1 channels is a mechanism for sub cellular regulation of mechanical sensitivity. *bioRxiv*. https://doi.org/10.1101/602532 (Preprint posted April 9, 2019).

Coste, B., J. Mathur, M. Schmidt, T.J. Earley, S. Ranade, M.J. Petrus, A.E. Dubin, and A. Patapoutian. 2010. Piezo1 and Piezo2 are essential components of distinct mechanically activated cation channels. *Science*. 330: 55–60. https://doi.org/10.1126/science.1193270

Cox, C.D., N. Bavi, and B. Martinac. 2019. Biophysical principles of ion-channel-mediated mechanosensory transduction. *Cell Rep.* 29:1–12. https://doi.org/10.1016/j.celrep.2019.08.075

Davis, M.A., R.C. Ireton, and A.B. Reynolds. 2003. A core function for p120-catenin in cadherin turnover. *J. Cell Biol.* 163:525–534. https://doi.org/10.1083/jcb.200307111

Eijkelkamp, N., J.E. Linley, J.M. Torres, L. Bee, A.H. Dickenson, M. Gringhuis, M.S. Minett, G.S. Hong, E. Lee, U. Oh, et al. 2013. A role for Piezo2 in EPAC1-dependent mechanical allodynia. *Nat. Commun.* 4:1682. https://doi.org/10.1038/ncomms2673

Fettiplace, R. 2017. Hair cell transduction, tuning, and synaptic transmission in the mammalian cochlea. *Compr. Physiol.* 7:1197–1227. https://doi.org/10.1002/cphy.c160049

Fettiplace, R., D.N. Furness, and M. Beurg. 2022. The conductance and organization of the TMC1-containing mechanotransducer channel complex in auditory hair cells. *Proc. Natl. Acad. Sci. USA*. 119:e2210849119. https://doi.org/10.1073/pnas.2210849119

Haber, A.L., M. Biton, N. Rogel, R.H. Herbst, K. Shekhar, C. Smillie, G. Burgin, T.M. Delorey, M.R. Howitt, Y. Katz, et al. 2017. A single-cell survey of the small intestinal epithelium. *Nature*. 551:333–339. https://doi.org/10.1038/nature24489

Haselwandter, C.A., Y.R. Guo, Z. Fu, and R. MacKinnon. 2022. Elastic properties and shape of the Piezo dome underlying its mechanosensory function. *Proc. Natl. Acad. Sci. USA*. 119:e2208034119. https://doi.org/10.1073/pnas.2208034119

Ireton, R.C., M.A. Davis, J. van Hengel, D.J. Mariner, K. Barnes, M.A. Thoreson, P.Z. Anastasiadis, L. Matrisian, L.M. Bundy, L. Sealy, et al. 2002. A novel role for p120 catenin in E-cadherin function. *J. Cell Biol.* 159: 465–476. https://doi.org/10.1083/jcb.200205115

Jia, Z., R. Ikeda, J. Ling, V. Viatchenko-Karpinski, and J.G. Gu. 2016. Regulation of Piezo2 mechanotransduction by static plasma membrane tension in primary afferent neurons. *J. Biol. Chem.* 291:9087–9104. https://doi.org/10.1074/jbc.M115.692384

Katsuta, E., K. Takabe, M. Vujcic, P.A. Gottlieb, T. Dai, A. Mercado-Perez, A. Beyder, Q. Wang, and M. Opyrchal. 2022. Mechano-sensing channel PIEZO2 enhances invasive phenotype in triple-negative breast cancer. *Int. J. Mol. Sci.* 23:9909. https://doi.org/10.3390/ijms23179909

Knutson, K.R., S.T. Whiteman, C. Alcaino, A. Mercado-Perez, I. Finholm, H.K. Serlin, S.S. Bellampalli, D.R. Linden, G. Farrugia, and A. Beyder. 2022. Intestinal enteroendocrine cells rely on ryanodine and IP(3) calcium store receptors for mechanotransduction. *J. Physiol.* 601:287–305. https://doi.org/10.1113/JP283383

le Duc, Q., Q. Shi, I. Blonk, A. Sonnenberg, N. Wang, D. Leckband, and J. de Rooij. 2010. Vinculin potentiates E-cadherin mechanosensing and is recruited to actin-anchored sites within adherens junctions in a myosin II-dependent manner. *J. Cell Biol.* 189:1107–1115. https://doi.org/10.1083/jcb.201001149

Lecuit, T., and A.S. Yap. 2015. E-cadherin junctions as active mechanical integrators in tissue dynamics. *Nat. Cell Biol.* 17:533–539. https://doi.org/10.1038/ncb3136

Lembrechts, R., I. Brouns, K. Schnorbusch, I. Pintelon, J.P. Timmermans, and D. Adriaensen. 2012. Neuroepithelial bodies as mechanotransducers in the intrapulmonary airway epithelium: Involvement of TRPC5. *Am. J. Respir. Cell Mol. Biol.* 47:315–323. https://doi.org/10.1165/rcmb.2012-0068OC

Lewis, A.H., and J. Grandl. 2020. Inactivation kinetics and mechanical gating of Piezo1 ion channels depend on subdomains within the cap. *Cell Rep.* 30:870–880.e2. https://doi.org/10.1016/j.celrep.2019.12.040

Liu, X., Y. Jia, Z. Wang, Z. Zhang, and W. Fu. 2022. A pan-cancer analysis reveals the genetic alterations and immunotherapy of Piezo2 in human cancer. *Front. Genet.* 13:918977. https://doi.org/10.3389/fgene.2022.918977

Marshall, K.L., D. Saade, N. Ghitani, A.M. Coombs, M. Szczot, J. Keller, T. Ogata, I. Daou, L.T. Stowers, C.G. Bönnemann, et al. 2020. PIEZO2 in sensory neurons and urothelial cells coordinates urination. *Nature*. 588: 290–295. https://doi.org/10.1038/s41586-020-2830-7

Mercado-Perez, A., and A. Beyder. 2022. Gut feelings: Mechanosensing in the gastrointestinal tract. *Nat. Rev. Gastroenterol. Hepatol.* 19:283–296. https://doi.org/10.1038/s41575-021-00561-y

Miranda, K.C., S.R. Joseph, A.S. Yap, R.D. Teasdale, and J.L. Stow. 2003. Contextual binding of p120ctn to E-cadherin at the basolateral plasma membrane in polarized epithelia. *J. Biol. Chem.* 278:43480–43488. https://doi.org/10.1074/jbc.M305525200

Na, T.Y., L. Schecterson, A.M. Mendonsa, and B.M. Gumbiner. 2020. The functional activity of E-cadherin controls tumor cell metastasis at multiple steps. *Proc. Natl. Acad. Sci. USA*. 117:5931–5937. https://doi.org/10.1073/pnas.1918167117

Nonomura, K., S.H. Woo, R.B. Chang, A. Gillich, Z. Qiu, A.G. Francisco, S.S. Ranade, S.D. Liberles, and A. Patapoutian. 2017. Piezo2 senses airway stretch and mediates lung inflation-induced apnoea. *Nature*. 541: 176–181. https://doi.org/10.1038/nature20793

Noordstra, I., M.D. Hermoso, L. Schimmel, A. Bonfim-Melo, D. Currin-Ross, C.N. Duong, J.M. Kalappurakkal, R.G. Morris, D. Vestweber, S. Mayor, et al. 2023. An E-cadherin-actin clutch translates the mechanical force of cortical flow for cell-cell contact to inhibit epithelial cell locomotion. *Dev. Cell*. 58:1748–1763.e6. https://doi.org/10.1016/j.devcel.2023.06.011

Noren, N.K., B.P. Liu, K. Burridge, and B. Kreft. 2000. p120 catenin regulates the actin cytoskeleton via Rho family GTPases. *J. Cell Biol.* 150:567–580. https://doi.org/10.1083/jcb.150.3.567

Ozawa, M., H. Baribault, and R. Kemler. 1989. The cytoplasmic domain of the cell adhesion molecule uvomorulin associates with three independent proteins structurally related in different species. *EMBO J.* 8:1711–1717. https://doi.org/10.1002/j.1460-2075.1989.tb03563.x

Ranade, S.S., S.H. Woo, A.E. Dubin, R.A. Moshourab, C. Wetzel, M. Petrus, J. Mathur, V. Bégay, B. Coste, J. Mainquist, et al. 2014. Piezo2 is the major transducer of mechanical forces for touch sensation in mice. *Nature*. 516:121–125. https://doi.org/10.1038/nature13980

Rao, J., C.T. Lim, T. Hu, and D. Han. 2021. Editorial: Cancer cell mechanobiology - a new frontier for cancer invasion and metastasis Research. *Front. Cell Dev. Biol.* 9:775012. https://doi.org/10.3389/fcell.2021.775012

Reynolds, A.B., J. Daniel, P.D. McCrea, M.J. Wheelock, J. Wu, and Z. Zhang. 1994. Identification of a new catenin: The tyrosine kinase substrate p120cas associates with E-cadherin complexes. *Mol. Cell Biol.* 14: 8333–8342.

Sadegh, S., J.L. Higgins, P.C. Mannion, M.M. Tamkun, and D. Krapf. 2017. Plasma membrane is compartmentalized by a self-similar cortical actin meshwork. *Phys. Rev. X.* 7:011031. https://doi.org/10.1103/PhysRevX.7.011031

Sako, Y., A. Nagafuchi, S. Tsukita, M. Takeichi, and A. Kusumi. 1998. Cytoplasmic regulation of the movement of E-cadherin on the free cell surface as studied by optical tweezers and single particle tracking: corralling and tethering by the membrane skeleton. *J. Cell Biol.* 140: 1227–1240. https://doi.org/10.1083/jcb.140.5.1227

Schneider, C.A., W.S. Rasband, and K.W. Eliceiri. 2012. NIH image to ImageJ: 25 years of image analysis. *Nat. Methods*. 9:671–675. https://doi.org/10.1038/nmeth.2089

Solé, L., and M.M. Tamkun. 2020. Trafficking mechanisms underlying Na_v channel subcellular localization in neurons. *Channels (Austin)*. 14:1–17. https://doi.org/10.1080/19336950.2019.1700082

Tamkun, M.M., K.M. O'connell, and A.S. Rolig. 2007. A cytoskeletal-based perimeter fence selectively corrals a sub-population of cell surface Kv2.1 channels. *J. Cell Sci.* 120:2413–2423. https://doi.org/10.1242/jcs.007351

Treichel, A.J., I. Finholm, K.R. Knutson, C. Alcaino, S.T. Whiteman, M.R. Brown, A. Matveyenko, A. Wegner, H. Kacmaz, A. Mercado-Perez, et al. 2022. Specialized mechanosensory epithelial cells in mouse gut intrinsic tactile sensitivity. *Gastroenterology*. 162:535–547.e13. https://doi.org/10.1053/j.gastro.2021.10.026

Twiss, F., Q. Le Duc, S. Van Der Horst, H. Tabdili, G. Van Der Krogt, N. Wang, H. Rehmann, S. Huveneers, D.E. Leckband, and J. De Rooij. 2012. Vinculin-dependent cadherin mechanosensing regulates efficient epithelial barrier formation. *Biol. Open*. 1:1128–1140. https://doi.org/10.1242/bio.20122428

Umans, B.D., and S.D. Liberles. 2018. Neural sensing of organ volume. *Trends Neurosci.* 41:911–924. https://doi.org/10.1016/j.tins.2018.07.008

van Roy, F. 2014. Beyond E-cadherin: Roles of other cadherin superfamily members in cancer. *Nat. Rev. Cancer*. 14:121–134. https://doi.org/10.1038/nrc3647

Verkest, C., I. Schaefer, T.A. Nees, N. Wang, J.M. Jegelka, F.J. Taberner, and S.G. Lechner. 2022. Intrinsically disordered intracellular domains

control key features of the mechanically-gated ion channel PIEZO2. *Nat. Commun.* 13:1365. https://doi.org/10.1038/s41467-022-28974-6

Wang, F., K. Knutson, C. Alcaino, D.R. Linden, S.J. Gibbons, P. Kashyap, M. Grover, R. Oeckler, P.A. Gottlieb, H.J. Li, et al. 2017. Mechanosensitive ion channel Piezo2 is important for enterochromaffin cell response to mechanical forces. *J. Physiol.* 595:79–91. https://doi.org/10.1113/JP272718

Wang, J., J. Jiang, X. Yang, G. Zhou, L. Wang, and B. Xiao. 2022. Tethering Piezo channels to the actin cytoskeleton for mechanogating via the cadherin-β-catenin mechanotransduction complex. *Cell Rep.* 38:110342. https://doi.org/10.1016/j.celrep.2022.110342

Wang, S., R. Chennupati, H. Kaur, A. Iring, N. Wettschureck, and S. Offermanns. 2016. Endothelial cation channel PIEZO1 controls blood pressure by mediating flow-induced ATP release. *J. Clin. Invest.* 126: 4527–4536. https://doi.org/10.1172/JCI87343

Woo, S.H., S. Ranade, A.D. Weyer, A.E. Dubin, Y. Baba, Z. Qiu, M. Petrus, T. Miyamoto, K. Reddy, E.A. Lumpkin, et al. 2014. Piezo2 is required for Merkel-cell mechanotransduction. *Nature*. 509:622–626. https://doi.org/10.1038/nature13251

Xu, K., G. Zhong, and X. Zhuang. 2013. Actin, spectrin, and associated proteins form a periodic cytoskeletal structure in axons. *Science*. 339: 452–456. https://doi.org/10.1126/science.1232251

Yang, X., C. Lin, X. Chen, S. Li, X. Li, and B. Xiao. 2022. Structure deformation and curvature sensing of PIEZO1 in lipid membranes. *Nature*. 604: 377–383. https://doi.org/10.1038/s41586-022-04574-8

Yao, M., W. Qiu, R. Liu, A.K. Efremov, P. Cong, R. Seddiki, M. Payre, C.T. Lim, B. Ladoux, R.M. Mège, and J. Yan. 2014. Force-dependent conformational switch of α-catenin controls vinculin binding. *Nat. Commun.* 5: 4525. https://doi.org/10.1038/ncomms5525

Zeng, W.Z., K.L. Marshall, S. Min, I. Daou, M.W. Chapleau, F.M. Abboud, S.D. Liberles, and A. Patapoutian. 2018. PIEZOs mediate neuronal sensing of blood pressure and the baroreceptor reflex. *Science*. 362:464–467. https://doi.org/10.1126/science.aau6324

Zhou, Z., X. Ma, Y. Lin, D. Cheng, N. Bavi, G.A. Secker, J.V. Li, V. Janbandhu, D.L. Sutton, H.S. Scott, et al. 2023. MyoD-family inhibitor proteins act as auxiliary subunits of Piezo channels. *Science*. 381:799–804. https://doi.org/10.1126/science.adh8190

Supplemental material

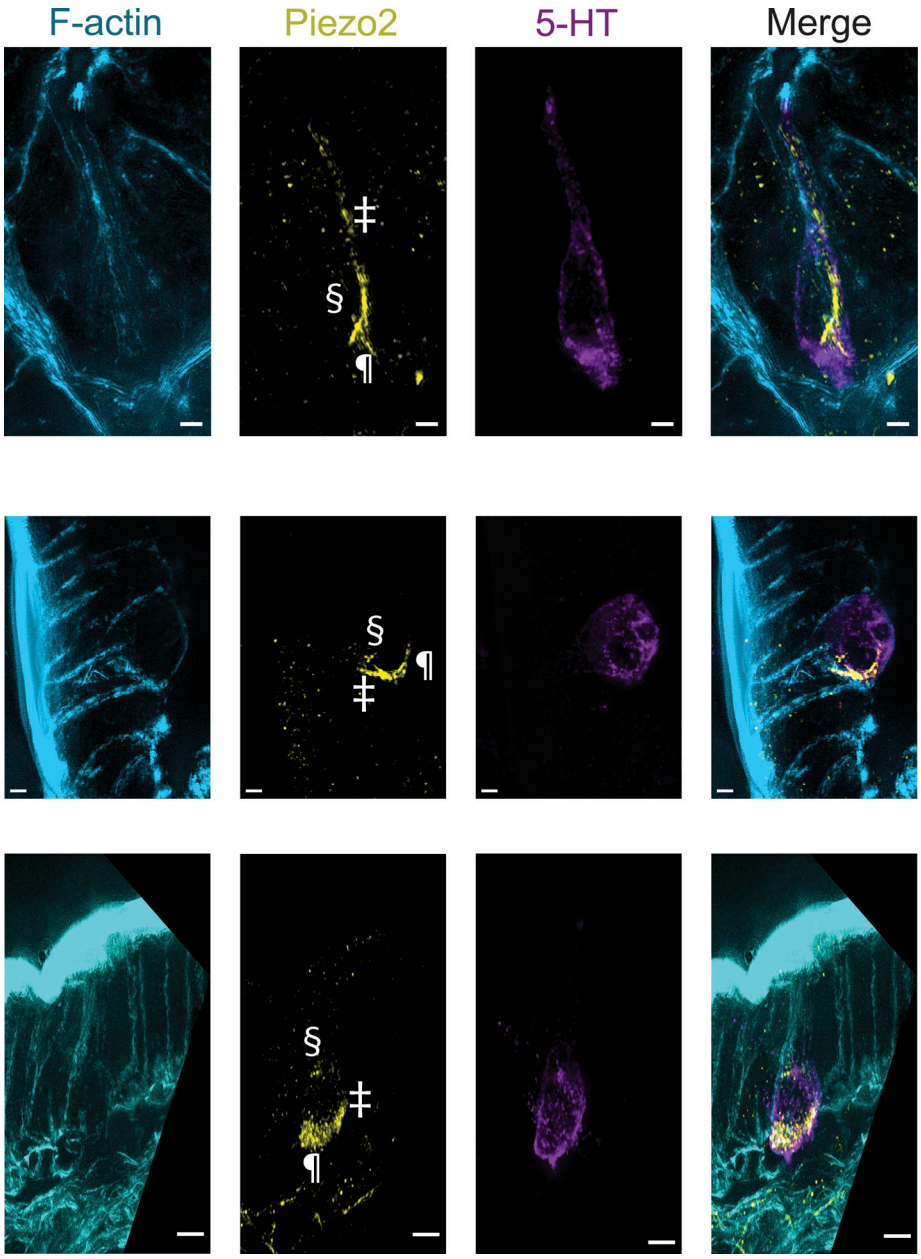

Figure S1. **Piezo2 localizes to three subcellular domains in GI epithelial mechanoreceptors.** Images from individual mice show that Piezo2 expression may be sorted into three general domains in mechanosensitive enterochromaffin cells: (1) lateral wall (‡), (2) basal cytoplasm (¶), and (3) perinuclear region (§). Scale bars: 2 µm.

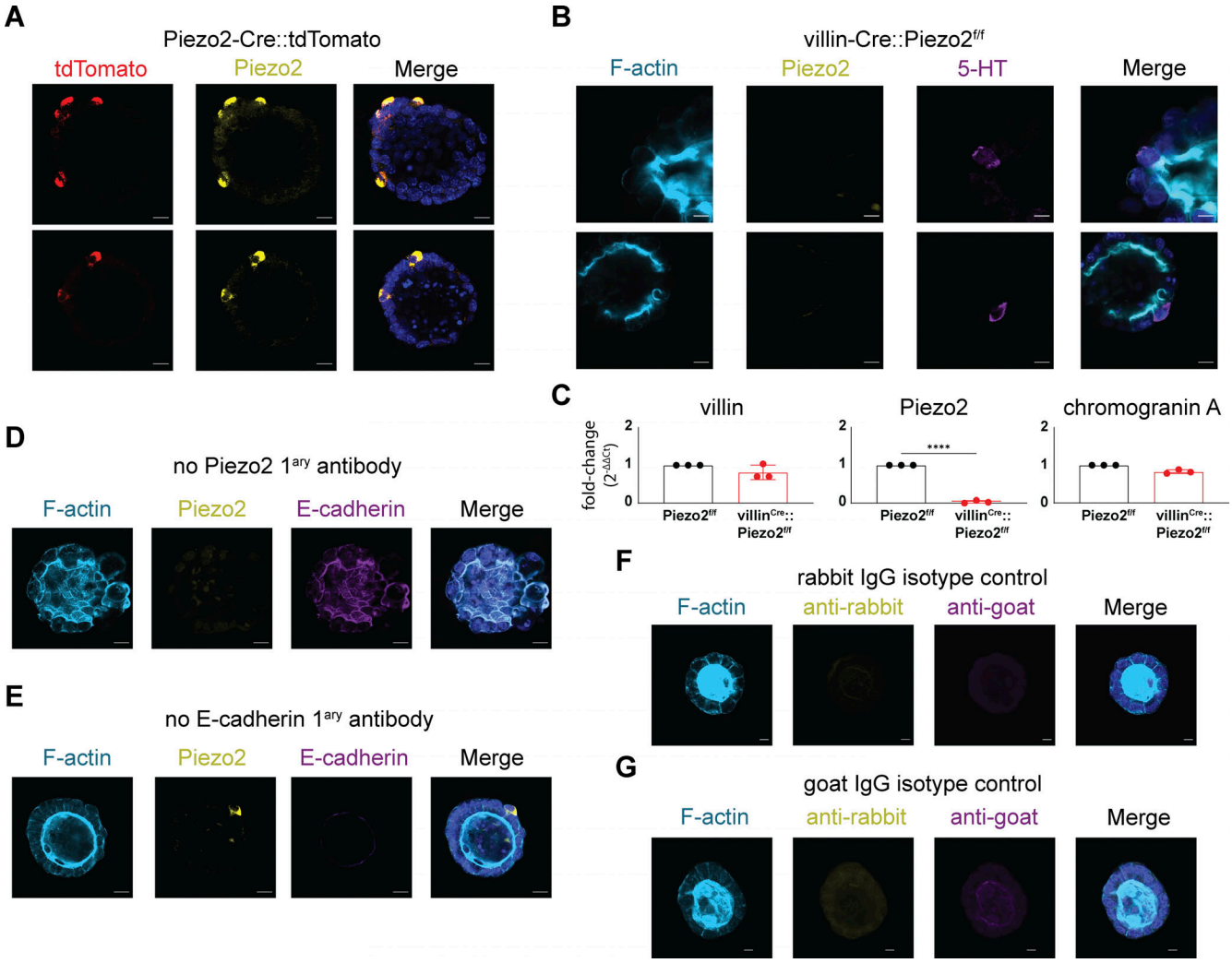

Figure S2. **Validation of anti-Piezo2 antibody and immunofluorescence approaches. (A)** Piezo2 antibody is specific for Piezo2-expressing cells. The Piezo2 antibody utilized in this manuscript for immunofluorescence (Novus biologicals NBP1-78624, Table 1) was used to image organoids from Piezo2-Cre::GCaMP5/tdTomato mice. Cytoplasmic fluorescence from the tdTomato reporter designates cells where Cre recombinase expression occurred downstream of Piezo2 expression and led to genetic recombination. Perfect overlap between tdTomato-expressing cells and those marked by the anti-Piezo2 antibody confirms antibody specificity. **(B)** Piezo2 antibody shows no off-target labeling. The Piezo2 antibody utilized in this manuscript for immunofluorescence (Novus biologicals NBP1-78624, Table 1) was used to image organoids from villin-Cre::Piezo2$^{f/f}$ mice. Villin is a pan-epithelial marker, so we expect no Piezo2 expression at all in these organoids. 5-HT staining allows us to identify enterochromaffin cells (a subset of EECs). The majority of these cells (Alcaino et al., 2018) should express the Piezo2 ion channel. The absence of Piezo2 signal in all 5-HT+ cells, plus the absence of signal in the rest of the epithelium, confirms a lack of off-target labeling. **(C)** To support the credibility of this approach in validating the Piezo2 antibody, we isolated mRNA from Piezo2$^{f/f}$ and villin-Cre::Piezo2$^{f/f}$ epithelial organoids and performed qRT-PCRs to calculate fold-changes in expression. We confirmed the absence of any Piezo2 transcript without changes in villin (pan-epithelial marker) nor chromogranin A (EEC marker) transcript levels. **(D and E)** Control immunofluorescence experiments without primary rabbit anti-Piezo2 (D) or primary goat anti-E-cadherin (E) antibody. **(F and G)** Control immunofluorescence experiments using rabbit (F) or goat (G) IgG isotype control antibodies in lieu of the primary antibodies. Phalloidin counterstain labels the F-actin architecture. Scale bars: 5 µm. ***P < 0.001 via an unpaired two-tailed Student's *t*-test.

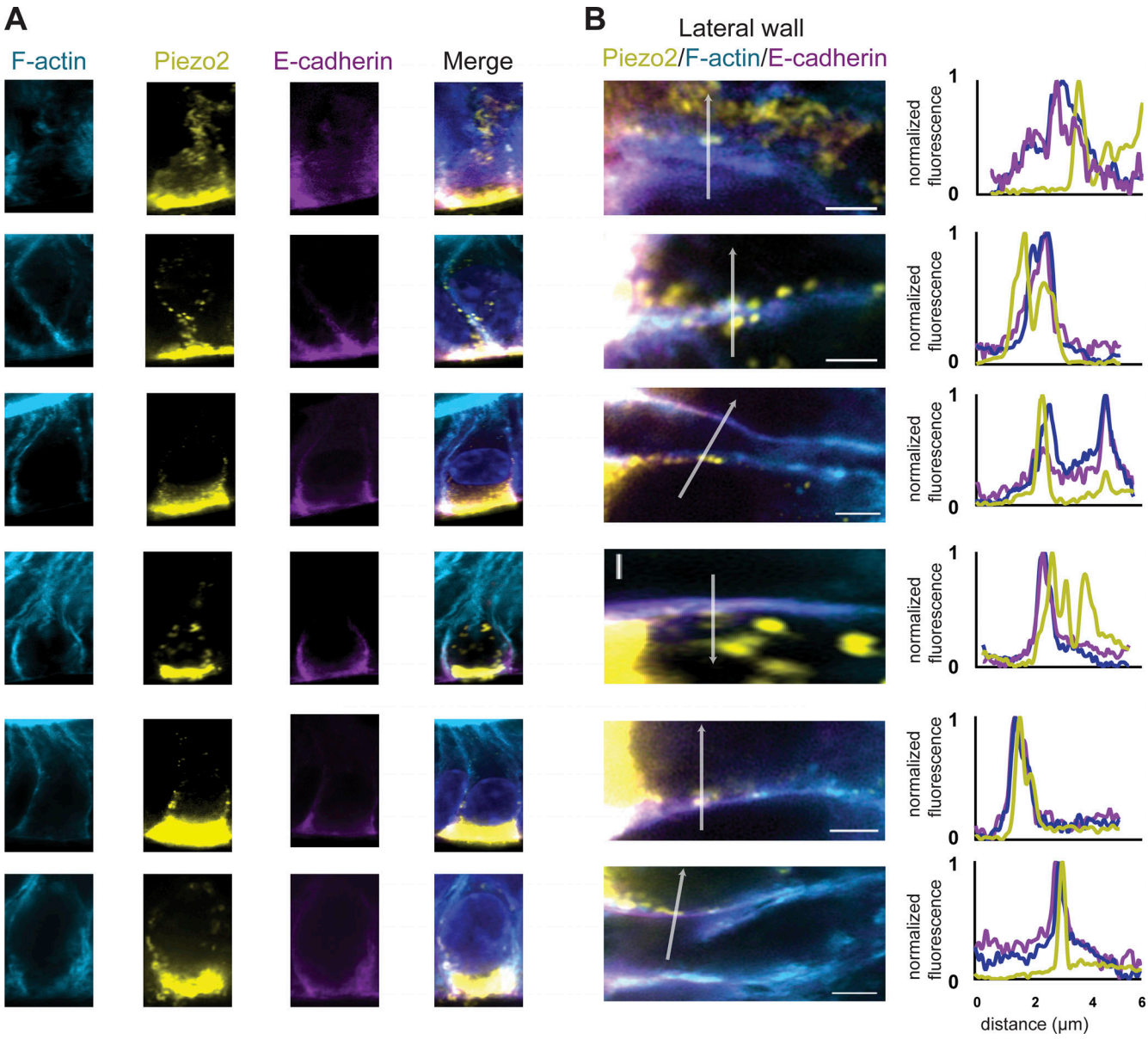

Figure S3. **Triple-labeling in intestinal organoids confirms Piezo2 localization patterns and its specific associations with actin and E-cadherin. (A)** Organoids derived from four different mice show similar localization patterns for Piezo2, F-actin, and E-cadherin. The same symbol convention (‡, ¶, §) as in Fig. 1 and Fig. 2 is used here. **(B)** Piezo2 localization at the lateral wall correlates with F-actin and E-cadherin labeling. Fluorescence profiles correspond to the line profile along the arrow in the images immediately to their left. Profiles are normalized to the average fluorescence intensity across the whole cell. Images in this figure were used to generate the graphs in Fig. 2 E. Scale bars: 5 μm (A), 2 μm (B).

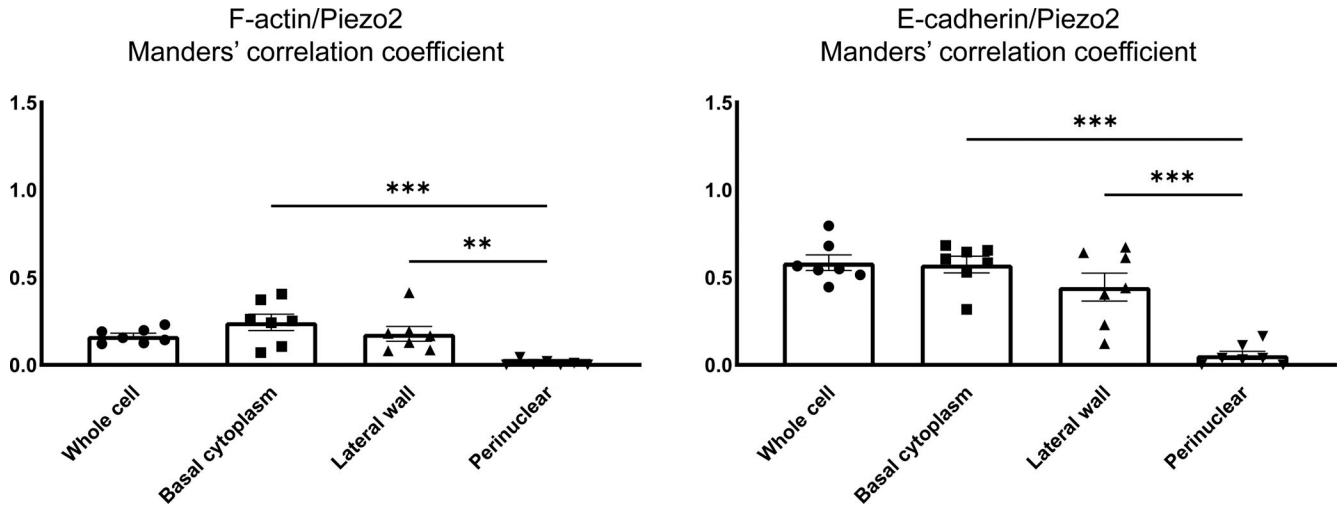

Figure S4. **Manders' correlation coefficients (MCCs) with Piezo2 in the denominator.** The MCC analyses in Fig. 2 also yield measurements of how much of the F-actin staining overlaps with Piezo2 immunofluorescence (left) and how much E-cadherin immunofluorescence overlaps with that of Piezo2 (right). F-actin/Piezo2 MCC: WC 0.16 ± 0.02, BC 0.24 ± 0.05, LW 0.18 ± 0.04, Pn 0.01 ± 0.01. E-cadherin/Piezo2 MCC: WC 0.58 ± 0.04, BC 0.54 ± 0.05, LW 0.44 ± 0.08, Pn 0.06 ± 0.02. **P < 0.01, ***P < 0.001.

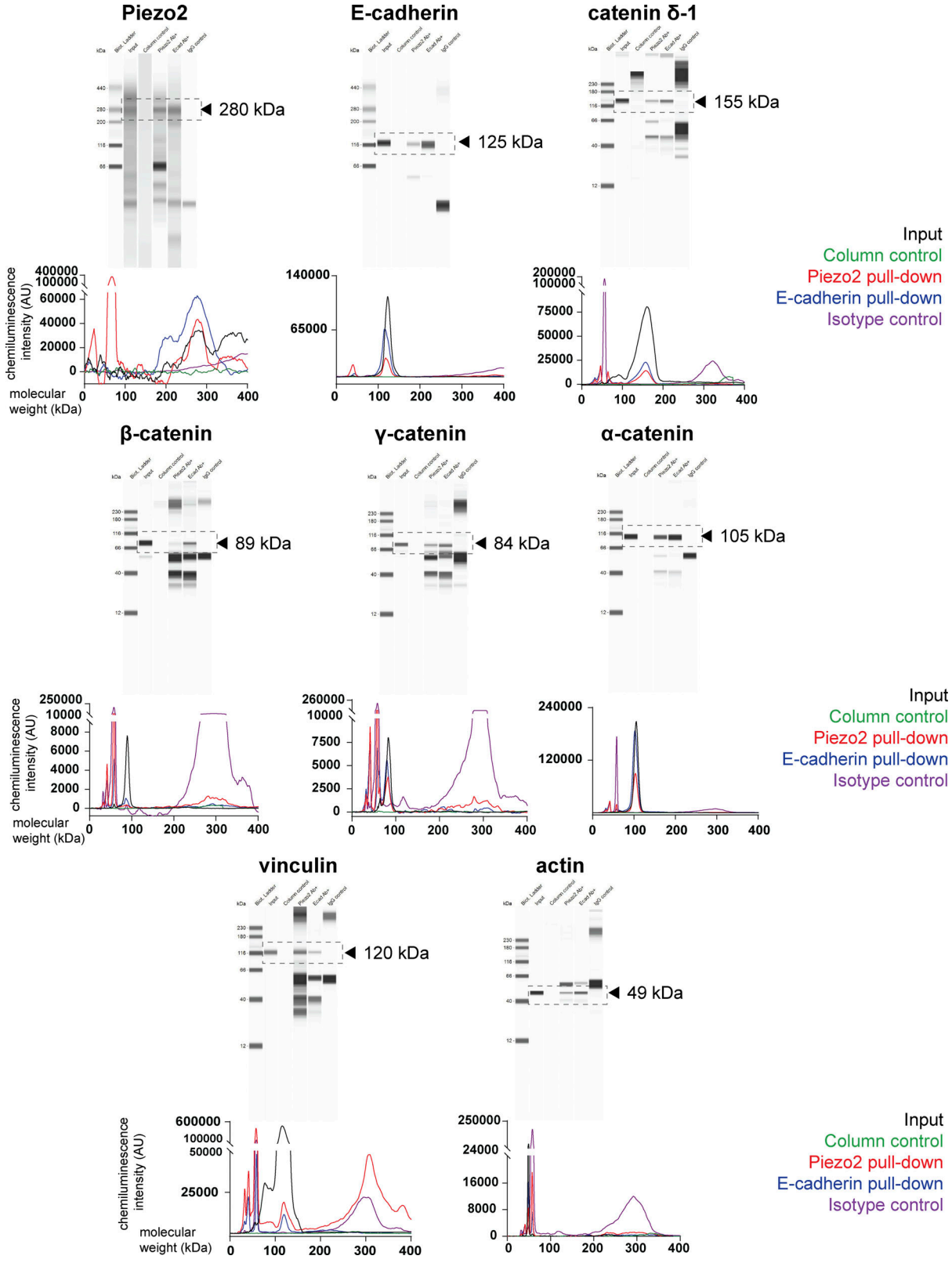

Figure S5. **Protein detection results.** Virtual "blots" generated by the Compass for Simple Western software. Dashed boxes correspond to cropped areas displayed in Fig. 2 that are centered around the molecular weight (MW) indicated to the right of the images. The thick band of ~55 kDa present in the Piezo2 pull-down, E-cadherin pull-down, and isotype control lanes corresponds to the heavy chain of the anti-Piezo2, anti-E-cadherin or IgG immunoglobulin utilized for pull-down, respectively. These antibodies had a rabbit host, like the primary detection antibodies of each experiment. Below each experiment is the electropherogram quantifying detection intensity across the MW range. Electropherogram profile colors correspond to samples indicated at the right of their rows. The areas under the correct MW peak in these and biological replicate experiments are plotted in Fig. 2 G.

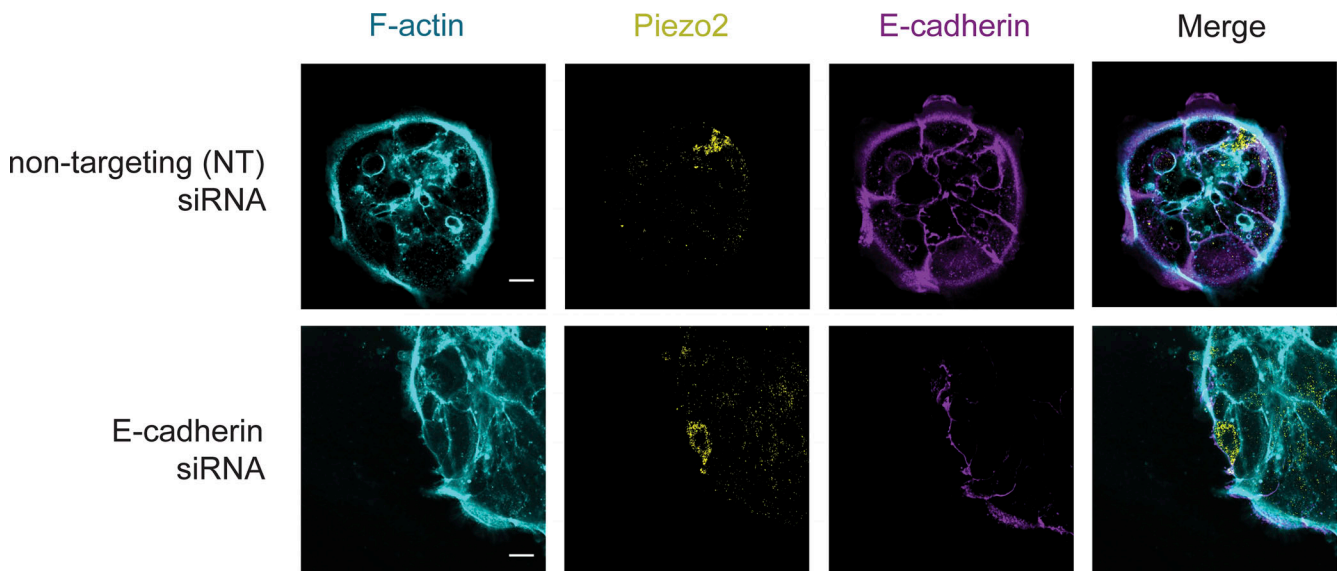

Figure S6. **Successful E-cadherin knockdown has no effect on Piezo2 expression.** Clusters of epithelial cells may coalesce into small monolayers when seeded onto planar substrates; these clusters also have a significantly higher probability of remaining attached to the plate after all the steps of immunostaining. Representative clusters are shown for cultures treated with NT or E-cadherin siRNA for 48 h. This was deemed appropriate to better interpret E-cadherin along the cell–cell borders. One cell in each cluster expresses Piezo2. No apparent changes are observed in the intensity or pattern of Piezo2 staining between NT and E-cadherin siRNA-treated cells, suggesting no changes in channel expression or trafficking. Scale bar: 10 µm.